Hindawi
Journal of Nanomaterials
Volume 2022, Article ID 9866111, 10 pages
https://doi.org/10.1155/2022/9866111

Research Article

Electrochemical Detection of H_2O_2 on Graphene Nanoribbons/Cobalt Oxide Nanorods-Modified Electrode

Preethika Murugan,[1] Ashok K. Sundramoorthy,[1] Ramila D. Nagarajan,[2] Raji Atchudan,[3] Rajeshkumar Shanmugam,[4] Dhanraj Ganapathy,[1] Sandeep Arya,[5] Asma A. Alothman,[6] and Mohamed Ouladsmane[6]

[1]*Centre for Nano-Biosensors, Department of Prosthodontics, Saveetha Dental College and Hospitals, Saveetha Institute of Medical and Technical Sciences, Poonamallee High Road, Velappanchavadi, Chennai, 600077 Tamil Nadu, India*
[2]*Department of Chemistry, V. V. Vanniaperumal College for Women, Virudhunagar, 626001 Tamil Nadu, India*
[3]*School of Chemical Engineering, Yeungnam University, Gyeongsan 38541, Republic of Korea*
[4]*Centre for Transdisciplinary Research, Department of Pharmacology, Saveetha Dental College, Saveetha Institute of Medical and Technical Sciences, Chennai, India*
[5]*Department of Physics, University of Jammu, Jammu, Jammu and Kashmir 180006, India*
[6]*Department of Chemistry, College of Science, King Saud University, Riyadh 11451, Saudi Arabia*

Correspondence should be addressed to Ashok K. Sundramoorthy; ashok.sundramoorthy@gmail.com

Received 12 May 2022; Revised 21 July 2022; Accepted 14 August 2022; Published 8 September 2022

Academic Editor: H C Ananda Murthy

The most important biological changes which have to be monitored is the mechanism of ageing in the human body where the mitochondria play a major role. Hydrogen peroxide (H_2O_2) is one of the important markers for the reactive oxygen species (ROS), which denatures the protein and DNA, that was the main contributory factor of ageing. So, it is very important to monitor H_2O_2 levels in the biological samples. Herein, we reported the preparation of 1D graphene nanoribbon/cobalt oxide nanorod (GNR/Co_3O_4) based nanocomposite-modified electrochemical sensor for H_2O_2. Firstly, GNR was synthesized by oxidative unzipping of multiwalled carbon nanotubes (MWCNTs). Secondly, cobalt oxide nanorods (Co_3O_4) were grown onto GNR by a chemical reduction process. As-prepared nanocomposite was characterized by UV-Visible spectroscopy (UV-Vis) and HR-TEM. Electrochemical properties of GNR/Co_3O_4-coated electrode were studied by cyclic voltammetry (CV) which showed two redox peaks at 0.93 and 0.88 V in phosphate buffer solution. Next, the electrocatalytic activity of GNR/Co_3O_4-coated electrode was studied against H_2O_2 oxidation. The electrochemical studies revealed that GNR/Co_3O_4-coated electrode exhibited high electrocatalytic activity for H_2O_2 oxidation at 0.925 V. This sensor showed a linear response for H_2O_2 oxidation from 10 to 200 μM. The limit of detection (LOD) was calculated to be 1.27 μM. The selectivity of the sensor was also studied with other biomolecules associated in the human body, and the results showed that interference effect is negligible. Thus, the proposed GNR/Co_3O_4-modified electrode can be used for H_2O_2 detection with excellent stability and selectivity.

1. Introduction

Hydrogen peroxide (H_2O_2) is a well-known oxidizing agent. The process of manufacturing of H_2O_2 and its applications in various sectors are well documented [1]. H_2O_2 has been used in different industrial applications such as environmental, textile, clinical, pharmaceutical, and food [2]. Also, the importance of H_2O_2 is reported in many biosynthetic reactions and immune cell activation process [3]. The majority of the biological reactions were catalyzed by different enzymes such as lactate oxidase, cholesterol oxidase, D-amino acid oxidase, glutamate oxidase, and lysine oxidase, which resulted in the formation of H_2O_2 as a by-product. Thereby, it acts as a reactive oxygen species (ROS) that can promote the denaturation of proteins and DNA by oxidative processes [4]. Though it has cytotoxic effects, it plays a vital

role in controlling the physiological process of immune cell activation and vascular remodelling [5]. H_2O_2 involves in enzymatic reactions and acts as an intermediate for the level of glucose, lactose, and cholesterol [6]. Generally, H_2O_2 can enter into our body through consumption of instant coffee, green tea, or black tea that can raise the H_2O_2 concentration level above 100 μM which may enter into the gastrointestinal tract [7]. According to the US National Institute for Occupational Safety and Health, the permitted exposure limit of H_2O_2 is 1 ppm based on time-weighted average, but if it reaches above the level of 75 ppm, that is dangerous to health and may lead to death [8]. The anomalous level of H_2O_2 production in the human body may lead to carcinogenesis and severe complications such as formation of cancer and heart attack [9]. Thus, there is a vital need for monitoring H_2O_2 concentrations in the biological and environmental samples [10]. The analysis of H_2O_2 was generally carried out by traditional analytical methods such as spectrophotometry [11], colorimetry [12], fluorimetry [13], and electrochemical methods [14–17]. Colorimetry and fluorimetry methods are considered to be expensive and may not be suitable for general laboratory use. Electrochemical sensing of H_2O_2 can be performed by enzymatic and nonenzymatic methods [18, 19]. Enzymatic electrochemical sensors are vulnerable to the environmental factors such as temperature, pressure, pH, and biological pathogens [20]. The above-stated problems can be neglected by using nonenzymatic electrochemical sensors [21]. Majumder et al. reported a nonenzymatic electrochemical sensor for H_2O_2 and hydrazine using 3D microsnowflake architectures of α-Fe_2O_3 [22]. In 2019, Liu et al. prepared an innovative electrochemical sensor for detection of H_2O_2 using the hollow CuO/polyaniline nanohybrid fibers which exhibited a good linear range, lowest LOD, high selectivity, and extended stability [23]. Baghayeri et al. have prepared magnetic graphene oxide functionalized with an amine-terminated material that showed excellent electrochemical activity against H_2O_2 in the linear range of 0.05 to 160 μM with LOD of 0.01 μM [24].

Recently, carbon nanomaterials such as carbon dots (0D), carbon nanotubes (1D) [25, 26], graphene (2D) [27, 28], and graphite (3D) [29, 30] have been exploited as electrode materials for various electrochemical applications [31, 32]. Graphene nanoribbons (GNR) is a narrow strip of graphene with a quasi one-dimensional structure, which holds complementary properties of graphene sheet [33]. From the theoretical analysis, GNR's electrical nature can be tuned by the size and edge formation, and they can differ from metallic to semiconducting nature [34, 35]. The physical properties of the GNR are based on the length, width, and number of layers, which in the sequence depends on their preparation process. There are three methods available for the preparation of GNR: (i) cutting graphene by using different lithographic techniques [36, 37], (ii) bottom-up synthesis from polycyclic molecules [38, 39], and (iii) unzipping of carbon nanotubes [40–42]. Although the bottom-up technique offers a method to definite edge control, the lithographic process can produce GNR with exact location. However, the unzipping process offers the benefit of bulk preparation of GNR on a large scale. GNR prepared by the unzipping process has been effectively used in many applications such as a catalyst support for lithium-ion batteries [43, 44]. Unzipping of multiwall carbon nanotubes (MWCNTs) are classified into four types: (a) the reductive intercalation-assisted method [45], (b) the oxidative unzipping [46], (c) the electrochemical unzipping [47], and (d) miscellaneous approaches [48]. The first method depends on the familiar capability of alkali compounds to interpolate by the expansion of graphite along the z-axis direction. This process of unzipping of MWCNTs creates lattice expansion tempts high strain within the concentrical walls, succeeding in the breaking or opening of longitudinal directions of the tubes [33]. Common intercalants such as lithium and potassium metals have been used [33] which produced GNR with high conductivity, but they persisted multilayered flakes. GNR cannot be separated into single-layer ribbons because of the attraction between the surfaces. The oxidative method comprises treating of MWCNTs in a lower pH environment with a preparation as similar to synthesis of graphene oxide from the natural graphite [49]. Pristine graphene has an inert chemical surface without defects, and they exhibited poor water solubility. On the contrary, as-prepared GNRs are more reactive. The high reactivity of GNRs are linked to the adsorption of analytes via $\pi - \pi$ stacking interaction and by electrostatic or hydrogen bonding interactions with functionalities of the target molecules or the oxygen moieties located at the edges of the graphene material [50].

The purpose of using nanomaterials in the fabrication of sensors is to increase the sensitivity, enhance catalytic activity of the process, reduce the over potentials, and increase the electron transfer rate of the reaction [51, 52]. Transitional metals mainly boost the oxidation of several substrates because they can initiate the process of multielectron oxidation [53]. Also, nanoscale compounds can improve diffusion and offers a good active surface for electrocatalytic reactions [54]. Cobalt oxide-based nanomaterials (Co_3O_4) have been used in energy storage, electrochromic thin films, magneto-resistive devices, and heterogeneous catalysis [55]. Additionally, Co_3O_4 remains an attractive catalyst, mainly due to its outstanding electrocatalytic activity against ozone and oxygen.

Herein, a nanocomposite made of 1D GNR/Co_3O_4 was prepared by the top-down method and then used to fabricate an electrochemical H_2O_2 sensor. Firstly, Co_3O_4 nanorods were synthesized by a chemical reduction process. Secondly, GNR was synthesized by oxidative unzipping of multiwalled carbon nanotubes (MWCNTs). Followed by, GNR/Co_3O_4 nanocomposite was prepared and characterized by UV-visible (UV-Vis) and HR-TEM. Electrochemical properties of GNR/Co_3O_4 were studied by cyclic voltammetry (CV) which showed two redox peaks centered at 0.93 and 0.88 V in phosphate buffer solution. Next, electrochemical oxidation of H_2O_2 was performed on GNR/Co_3O_4-modified electrode. Further, the electrochemical studies were revealed that the H_2O_2 oxidation occurs at 0.925 V. By using CV, the linear response of the sensor was obtained from 10 to 200 μM H_2O_2, and LOD was calculated as 1.27 μM. The selectivity of the sensor was also studied for H_2O_2 oxidation in the presence of other biomolecules. It was concluded that

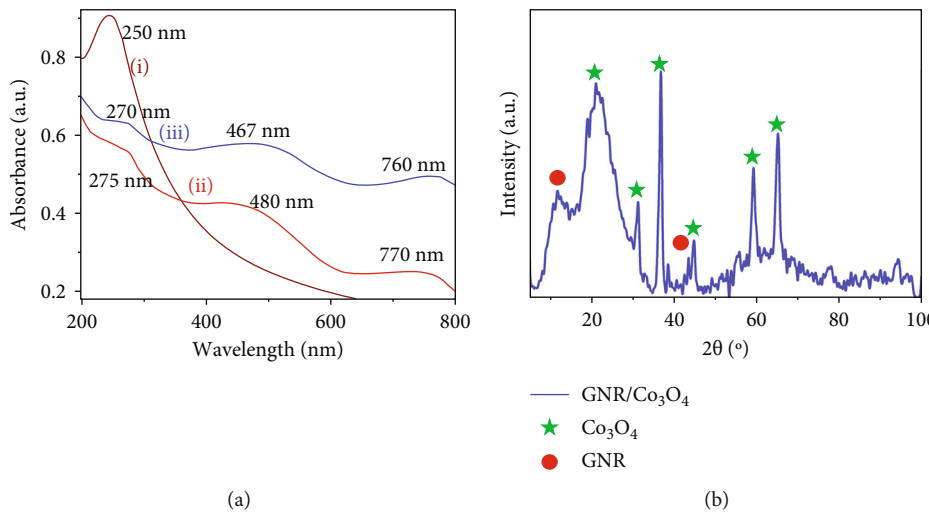

Figure 1: (a) UV–Vis spectra of (i) GNR, (ii) Co_3O_4 nanorods, and (iii) GNR/Co_3O_4 dispersions. (b) XRD spectrum of GNR/Co_3O_4 film.

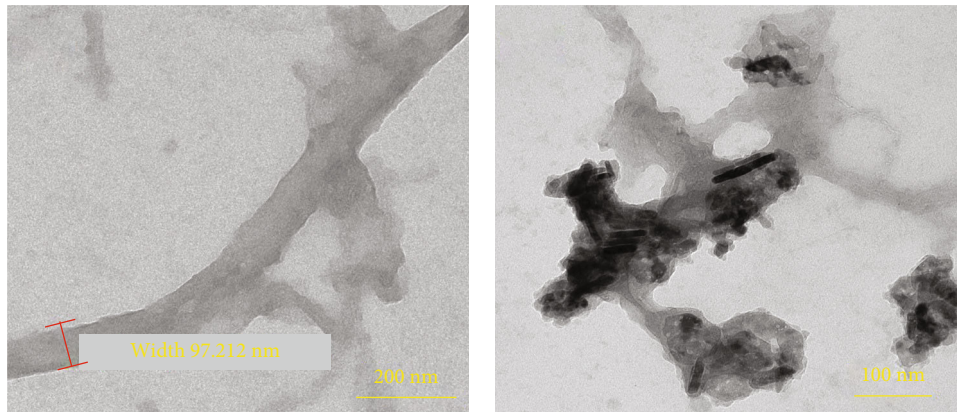

Figure 2: HR-TEM images of (a) GNR and (b) GNR/Co_3O_4 nanocomposite dispersions.

the proposed GNR/Co_3O_4-modified electrode could be used for selective detection of H_2O_2.

2. Experimental

2.1. Materials and Methods. Cobalt nitrate hexahydrate, MWCNTs, sodium hydroxide, and ascorbic acid (AA) were obtained from Sigma-Aldrich, India. Sulphuric acid, H_2O_2, uric acid (UA), paracetamol (PA), glucose, lactose, L-isoleucine, L-tyrosine, and potassium permanganate ($KMnO_4$) purchased from SRL, India. The phosphate buffer electrolyte solution was prepared using NaH_2PO_4 and Na_2HPO_4 (pH = 7.4) for the sensing of H_2O_2. All the chemicals were of analytical grade and used without any further purifications. All the solutions were prepared with the milli-Q-water (18.2 MΩ.cm @ 25 ± 2°C). Electrochemical studies were carried out using a three-electrode system with an electrochemical workstation (Model: CHI-760E, USA). UV-Vis spectra of GNR/Co_3O_4 nanocomposite was recorded using 2000c nanodrop spectrophotometer, Nanodrop Technologies, USA. All the experiments were done at room temperature (25 ± 0.2°C). The surface morphology of GNR/Co_3O_4 was examined by high-resolution transmission electron microscope (HR-TEM) (Model: 2100, JEOL, Japan). Samples for HR-TEM were prepared by coating of GNR/Co_3O_4 dispersion on the copper grid and dried in a vacuum oven at room temperature.

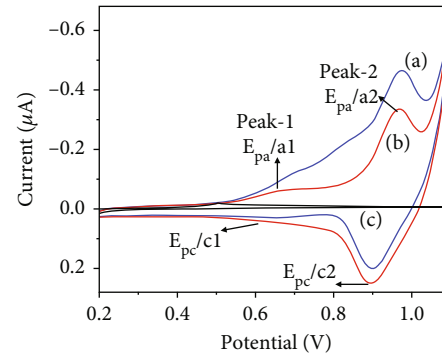

Figure 3: CVs of GNR/Co_3O_4/GCE were recorded in the absence (curve b) and presence of 30 μM H_2O_2 (curve a) in 0.1 M PBS (pH 7.4). CVs were also recorded using a bare GCE in 0.1 M PBS (pH 7.4) with 30 μM H_2O_2 (curve c). Scan rate = 50 mV/s.

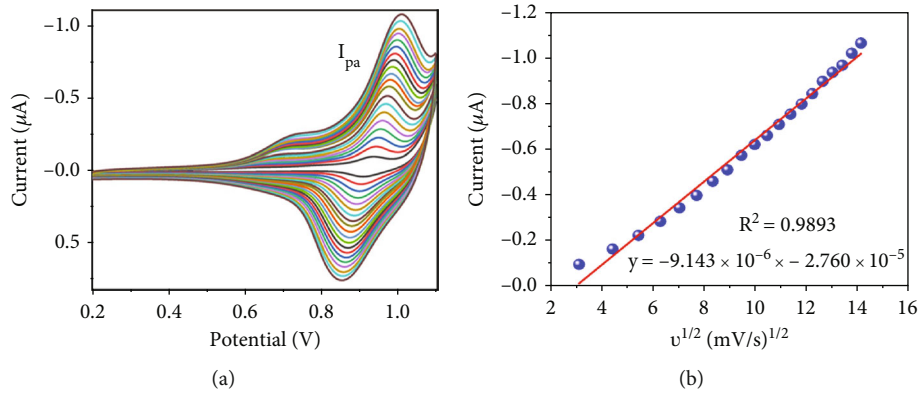

Figure 4: (a) CVs were recorded at different scan rates from 10 to 200 mV/s using a GNR/Co_3O_4/GCE in 0.1 M PBS (pH 7.4) containing 30 μM H_2O_2. (b) A linear plot was made between oxidation peak currents of H_2O_2 and square root of scan rates.

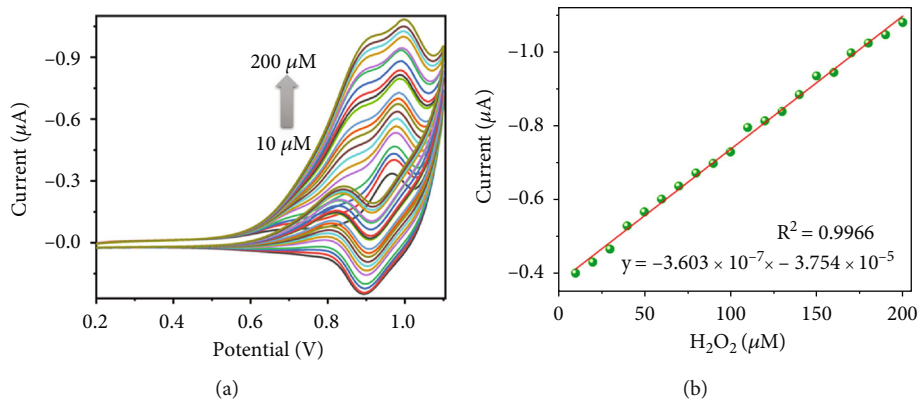

Figure 5: (a) CVs of GNR/Co_3O_4/GCE were recorded in 0.1 M PBS (pH 7.4) at a scan rate of 50 mV/s with successive additions of 10 μM of H_2O_2 in the range from 10 to 200 μM. (b) A linear calibration plot was made between I_{pa} vs. [H_2O_2].

2.2. Synthesis of GNR by Unzipping of MWCNTs. 0.025 g of MWCNTs was mixed with 7.5 mL of conc. sulfuric acid and then constantly stirred using a magnetic stirrer for 3 h at room temperature. After that, 0.125 g of potassium permanganate ($KMnO_4$) was added, and then, solution temperature was maintained at below 10°C using an ice-bath for 2 h. After that, the temperature was increased up to 35°C for 30 min. and then further increased up to 75°C for the next 30 min. Finally, this mixture was added in to 300 mL of ice water containing 10 mL of 30% H_2O_2 and filtered. After that, the reaction mixture washed with distilled water until the solution pH reaches neutral. As-synthesized GNR was filtered and dried in the vacuum oven at 60°C for 10 h [56].

2.3. Synthesis of GNR/Co_3O_4 Nanorods Nanocomposite. Sodium hydroxide (2.0 M, 5.0 mL) solution was added into the cobalt nitrate hexahydrate solution (0.01 M, 50 mL). In this step, the color of the solution turned into pale pink and then dark pinkish brown. 5 mL of GNR (0.1 mg/mL) aqueous dispersion was added into the pinkish-brown solution which turned as a dark black dispersion. After stirring for 0.5 h, AA solution (0.6 M, 5.0 mL) was added drop-wise into the solution. The black color liquid was slowly formed which was stirred for 3 h at 55°C. The precipitate was collected by centrifugation and washed with distilled water to remove the impurities and finally dried in a vacuum oven at 60°C for 5 h. Additionally, the prepared GNR/Co_3O_4 nanocomposite was calcinated for 2 h at 300°C.

2.4. Preparation of GNR/Co_3O_4/GCE. Initially, GCE was polished on a polishing pad with the sequence of alumina powder (Al_2O_3, sizes with ~1 μm, ~0.3 μm, and ~0.05 μm). Next, the GCE was washed with ultrapure Milli-Q water and left to air-dry at room temperature. After that, 10 μL of homogeneous GNR/Co_3O_4 (1 mg/mL) nanocomposite dispersion was drop casted on the electrode surface and left to dry. To discard the unbounded particles, the GNR/Co_3O_4/GCE was rinsed with distilled water. In the same manner, GNR/GCE and Co_3O_4/GCE were prepared for the control experiments.

3. Results and Discussion

3.1. UV-Visible Spectroscopy. UV–Vis spectra of GNR dispersion showed a strong absorbance band at 250 nm, which denoted the $\pi - \pi^*$ transition of aromatic C=C bonds, that was assigned to the partially oxidized graphene (Figure 1(a), curve i) [57]. Figure 1(a) (curve ii) shows the absorbance bands for Co_3O_4 nanorods at 275 and 480 nm which denoted the charge transfer from ($O^{2-} \rightarrow Co^{2+}$ and $O^{2-} \rightarrow Co^{3+}$) [58]. The broad peak found at 770 nm can be assigned to the d-d transition band from $^4A_2$ (F) $\rightarrow$ $^4T_1$ (p) transition of Co^{2+}

Table 1: The comparison of the various reported electrochemical H_2O_2 sensors with the proposed method.

S. no.	Electrode modification	Linear range (μM)	LOD (μM)	References
1	GS-PSS/GRCAPS	10-12000	3.3	[63]
2	rGO–Fe_2O_3	50-9000	6	[64]
3	Co_3O_4 –rGO	15-675	2.4	[65]
4	GNR/Co_3O_4/GCE	10-200	1.27	This work

G: graphene; PSS: poly(sodium 4-styrenesulfonate); GRCAPS: graphene capsules; rGO: reduced graphene oxide; Fe_2O_3: iron oxide.

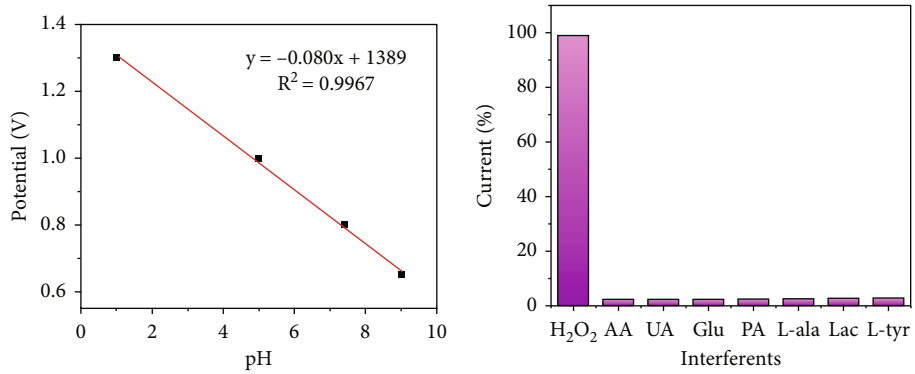

Figure 6: (a) A linear plot was made between the pH vs. redox potential of GNR/Co_3O_4/GCE. CVs were recorded in different pH (1, 5, 7.4, and 9) buffer solutions using a GNR/Co_3O_4/GCE. (b) Bar diagram shows the variations in the obtained current response (%) of 10 μM H_2O_2 after additions of 10 μM of AA, UA, glucose, PA, L-alanine, lactose, and L-tyrosine.

[58]. Figure 1(a) (curve iii) shows the absorbance spectrum of GNR/Co_3O_4 nanocomposite, where cobalt charge transfer peaks were blue shifted and observed at 270 and 467 nm. The peak shift was also observed in the d-d transition peak at 760 nm, indicating that composite was formed successfully. Next, the XRD patterns of the GNR/Co_3O_4 nanocomposite was recorded as shown in Figure 1(b). GNRs exhibited a peak at 2θ of 11.9°, which confirmed the unzipping of MWCNTs, and confirmed the successful formation of GNR sheets [59]. The XRD peaks of MWCNTs were diminished and disappeared at 25.8° and 44° [60]. The other XRD bands were observed at $2\theta = 20.2°$ (111), 30.7° (220), 38.6° (311), 44.8° (400), 58.7° (511), and 65.38° (440), which indicated the presence of Co_3O_4 [61].

3.2. HR-TEM. Figures 2(a) and 2(b) show the HR-TEM images of (a) GNR and (b) GNR/Co_3O_4 nanocomposite. GNR dispersion showed the unzipped MWCNTs clearly with the breadth of 97.2 nm. The GNR could be observed with few ribbons overlapped with each other as shown in Figure 2(a). Interestingly, for the nanocomposite film, Co_3O_4 nanorods were decorated on the surface of GNRs which can be observed from TEM image of GNR/Co_3O_4 nanocomposite.

3.3. Electrochemical Oxidation of H_2O_2. Electrochemical activities of GNR/Co_3O_4-modified GCE and bare GCE were performed by cyclic voltammetry (CV). GNR/Co_3O_4/GCE exhibited two redox peaks. In the first anodic scan, two oxidation peaks a1 and a2 were observed at 0.68 V and 0.93 V. In the reverse scan, two cathodic peaks (c1 and c2) were observed at 0.65 V and 0.88 V, respectively. The formal

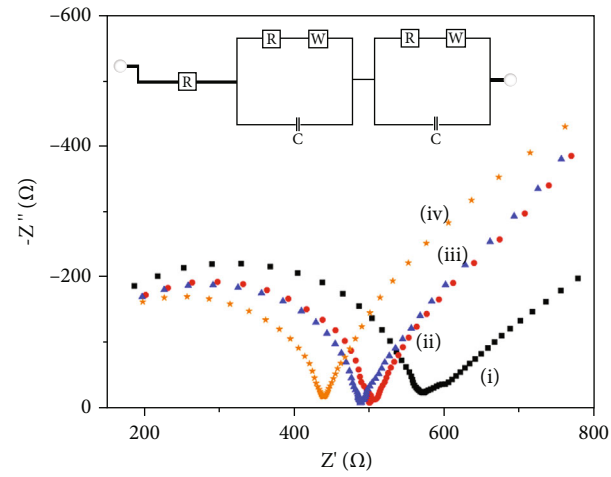

Figure 7: The Nyquist plots were recorded using (i) bare GCE, (ii) GNR/GCE, (iii) Co_3O_4 nanorods, and (iv) GNR/Co_3O_4/GCE in 0.1 M KCl with 5 mM $[Fe(CN)_6]^{3-/4-}$ by applying an AC voltage with 5 mV amplitude in a frequency range from 100 MHz to 100 kHz.

potential of the two redox peaks were found to be 0.665 V (peak I) and 0.905 V (peak II) (Figure 3 curve b). Cobalt oxide-modified electrode showed two pairs of redox peaks due to the Co(II)/Co(III) transition at the GCE surface as given in Equation (1) [62]. Electrocatalytic activity of the GNR/Co_3O_4-modified GCE (Figure 3, curve a) was recorded in 0.1 M phosphate buffer solution (PBS) containing 30 μM H_2O_2. Due to the high electrocatalytic activity of the GNR/Co_3O_4/GCE, oxidation peak of Co_3O_4 was enhanced due

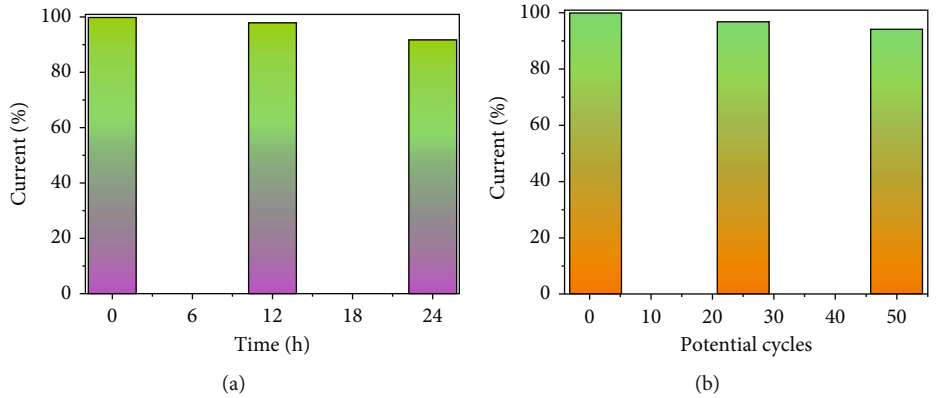

Figure 8: (a) The repeatability of GNR/Co_3O_4/GCE tested with 30 μM H_2O_2 after storage for different periods of time. (b) Stability study of GNR/Co_3O_4/GCE in PBS up to 50 CV cycles, scan rate = 50 mV/s.

Table 2: Electrochemical analysis of spiked H_2O_2 concentrations in an antiseptic solution using GNR/Co_3O_4/GCE.

S. no.	Samples	Added (μM)	Found (μM)	RSD (%)	Recovery (%)
1	Antiseptic solution with spiked H_2O_2	40	38.7	4.01	96.75
2	Antiseptic solution with spiked H_2O_2	50	49.1	3.61	98.20
3	Antiseptic solution with spiked H_2O_2	60	59.76	3.26	99.60

to H_2O_2 oxidation at 0.925 V (Figure 3 curve a) Equation (2). For comparison, CVs of bare GCE was recorded from 0.2 to 1.1 V at the scan rate of 50 mV/s (Figure 3, curve c). Bare GCE showed only the nonfaradic current, which clearly indicated that GNR/Co_3O_4-modified GCE had more electrocatalytic activity. The surface coverage of the GNR/Co_3O_4-modified electrode was calculated using Equation (3),

$$Co_3O_4 + H_2O + OH^- \longrightarrow 3CoOOH + e^- \quad (1)$$

$$6CoOOH + H_2O_2 \longrightarrow 2Co_3O_4 + O_2 + 4H_2O \quad (2)$$

$$I_p = \frac{n^2 F^2 \nu A r}{4RT} \quad (3)$$

where n is the number of electrons ($n = 2$), F is the faraday constant, R is the gas constant, A is the area of the electrode (0.0707 cm^2), and T is the temperature [6]. From the slope of the graph between H_2O_2 oxidation current and square roots of scan rate (Figure 4), the surface coverage ($r_{GNR/Co3O4}$) of the electrode was calculated as 0.32×10^{-10} mol/cm^2.

To ascertain about the effects of scan rate, CVs of GNR/Co_3O_4/GCE were recorded in 0.1 M PBS containing 30 μM H_2O_2 with different scan rates (Figure 4(a)). The anodic peak currents of GNR/Co_3O_4/GCE were increased linearly with the increase of the scanning rate from 10 to 200 mV/s. The linear equation was established between H_2O_2 oxidation peak currents and square root of scan rates with a correlation coefficient of (R^2) 0.9893 (Figure 4(b)). It was found that H_2O_2 oxidation on GNR/Co_3O_4/GCE was a diffusion-controlled process [18].

Next, electrocatalytic oxidation of H_2O_2 on the GNR/Co_3O_4/GCE-modified electrode was studied in 0.1 M PBS by varying the concentrations. The oxidation peak of H_2O_2 takes place at the oxidation potential of Co^{3+} (0.925 V) with each addition of 10 μM of H_2O_2. H_2O_2 oxidation peak currents were increased linearly from 10 to 200 μM (Figure 5(a)). Hence, a calibration plot was made between the concentration of H_2O_2 and the oxidation peak currents, which resulted in a linear equation of $Y = -3.603 \times 10^{-7}x - 3.754 \times 10^{-5}$ and (R^2) of 0.9966 (Figure 5(b)).

This data confirmed that GNR/Co_3O_4 can be used as an appropriate electrocatalyst for the analysis of H_2O_2. The limit of detection (LOD) was estimated as 1.27 μM. The sensitivity of the sensor was calculated as 5.10 $\mu A\, \mu M^{-1}\, cm^{-2}$. We have also compared the analytical performance of this new sensor with other reported sensors in Table 1. It was clear that this new sensor is more promising than some of the reported H_2O_2 sensors.

3.4. Effect of pH and Interferent Studies on GNR/Co_3O_4/GCE. GNR/Co_3O_4/GCE was subjected to study the effect of pH. CVs were recorded in different pH electrolyte solutions (from pH 1 to 9). It was found that the redox peak II of GNR/Co_3O_4/GCE was pH dependent which showed that protons are involved in the electron-transfer process. Figure 6(a) shows the linear plot of $E^{o'}$ vs. pH which gave a slope value of -80 mV/pH. This indicated that an unequal number of protons and electrons were involved in the electrochemical reactions [66]. For the electrochemical detection of H_2O_2, pH 7.4 was chosen as an appropriate electrolyte because of the physiological condition of the solutions.

The interferents analysis was carried out in the presence of H_2O_2 using the GNR/Co_3O_4/GCE. In this study, various common interfering biomolecules associated with the human body such as AA, PA, UA, glucose, lactose, L-isoleucine, and L-tyrosine were added (10 μM of each compound) with the analysis of 10 μM H_2O_2 (Figure 6(b)) [67]. These interfering molecules did not show any significant response

on the GNR/Co_3O_4/GCE. Therefore, it was suggested that GNR/Co_3O_4/GCE may be used for selective analysis of H_2O_2 by electrochemical oxidation.

3.5. Electrochemical Impedance, Repeatability, and Stability Studies. Electrochemical impedance spectroscopy (EIS) could reveal about the solid–liquid interface process of the modified electrodes. Figure 7 shows Nyquist plots obtained for (i) bare GCE, (ii) GNR/GCE, (iii) Co_3O_4/GCE, and (iv) GNR/Co_3O_4/GCE in 0.1 M KCl containing 5 mM $[Fe(CN)_6]^{3-/4-}$. The Nyquist impedance spectra obtained for (i) bare GCE (580 Ω), (ii) GNR/GCE (500 Ω), (iii) Co_3O_4/GCE (490 Ω), and (iv) GNR/Co_3O_4/GCE (425 Ω) indicated the charge transfer resistance (Rct) of each electrode by various diameters of semicircles [16]. For bare GCE, a small semicircle was found with the resistance of 580 Ω due to good electron transfer process. However, after modification with GNR/GCE layer, the electron transfer resistance was slightly decreased to 500 Ω, and Co_3O_4/GCE showed Rct of about 490 Ω. Interestingly, as-prepared nanocomposite showed the lowest Rct of about 425 Ω [68, 69], which indicated the high conductivity of GNR in the nanocomposite. As shown in the inset of Figure 7, an equivalent electrical circuit model was prepared and fitted with the EIS data of GNR/Co_3O_4/GCE. In addition, this sensor retained 93% of the electrode response after 24 h of usage (Figure 8(a)) due to good stability of the materials. The repeatability of the GNR/Co_3O_4/GCE sensor was also tested with 30 μM H_2O_2. This new sensor response was only decreased about 5.4% after 50 potential cycles (Figure 8(b)).

3.6. Real Sample Analysis. The real-world sample analysis was carried out using a GNR/Co_3O_4/GCE sensor. In order to measure the concentration of H_2O_2 in a real-world sample, a commercial antiseptic sample was diluted for 10 times in phosphate buffer solution and spiked with 40, 50, and 60 μM of H_2O_2. These samples were analyzed by CV using a GNR/Co_3O_4/GCE sensor. The obtained results are shown in Table 2. The relative standard deviation (RSD) values for the detection of spiked H_2O_2 in three different samples were found to be 4.01%, 3.61%, and 3.26%. Also, the recoveries of spiked H_2O_2 were calculated using the same method, and the values were found in the range of 96.75 to 99.60%. Therefore, the above results indicated that H_2O_2 can be effectively determined in a real-world sample using GNR/Co_3O_4/GCE sensor. We believe that this new method can be adopted for the detection of H_2O_2 in various samples from the environmental and medical fields.

4. Conclusion

In this work, GNR was synthesized by unzipping of MWCNTs, and the Co_3O_4 nanorods were synthesized by AA as a reducing agent in alkaline condition. After that, GNR/Co_3O_4 nanocomposite was successfully prepared and used to modify the surface of GCE. UV-Vis and HR-TEM results showed the successful formation of Co_3O_4 nanorods on the GNR. The electrooxidation of H_2O_2 on the GNR/Co_3O_4-modified electrode taken place at the potential of 0.93 V. Furthermore, GNR/Co_3O_4 nanocomposite-coated GCE was successfully applied for the detection of H_2O_2 with high sensitivity and selectivity. The effect of scan rate on H_2O_2 oxidation at GNR/Co_3O_4 indicated the diffusion-controlled electrochemical process. Using CV, the linear range of H_2O_2 concentration was observed from 10 to 200 μM, and the LOD was estimated as 1.27 μM. The selectivity of the sensor was also studied in the presence of other biomolecules; it was confirmed that GNR/Co_3O_4-modified electrode may be used for selective detection of H_2O_2 with lower LOD.

Data Availability

The research data used to support the findings of this study are included in the article.

Disclosure

This research work was presented as an abstract at the International Conference on Technologies for Smart Green Connected Society, 2021 (SPAST Abstracts, 1(01); https://spast.org/techrep/article/view/1369).

Conflicts of Interest

The authors declare that they have no conflicts of interest.

Authors' Contributions

Preethika Murugan, Ashok K. Sundramoorthy, and Raji Atchudan contributed equally to this work.

Acknowledgments

AKS thanks the Science and Engineering Research Board (SERB) for funding through CRG/2021/001517. We thank the Department of Science and Technology (DST) (International Bilateral Cooperation Division), India, for financial support through "INDO-RUSSIA Project (File No. INT/RUS/RFBR/385)." This work was also funded by the Researchers Supporting Project number (RSP-2021/243), King Saud University, Riyadh, Saudi Arabia.

References

[1] S. C. Perry, D. Pangotra, L. Vieira et al., "Electrochemical synthesis of hydrogen peroxide from water and oxygen," *Nature Reviews Chemistry*, vol. 3, no. 7, pp. 442–458, 2019.

[2] S. Chen, R. Yuan, Y. Chai, and F. Hu, "Electrochemical sensing of hydrogen peroxide using metal nanoparticles: a review," *Microchimica Acta*, vol. 180, no. 1-2, pp. 15–32, 2013.

[3] S. F. Erttmann and N. O. Gekara, "Hydrogen peroxide release by bacteria suppresses inflammasome-dependent innate immunity," *Nature Communications*, vol. 10, no. 1, pp. 1–13, 2019.

[4] S. K. Maji, S. Sreejith, A. K. Mandal, X. Ma, and Y. Zhao, "Immobilizing gold nanoparticles in mesoporous silica covered reduced graphene oxide: a hybrid material for cancer cell detection through hydrogen peroxide sensing," *ACS Applied Materials & Interfaces*, vol. 6, no. 16, pp. 13648–13656, 2014.

[5] E. A. Veal, A. M. Day, and B. A. Morgan, "Hydrogen peroxide sensing and signaling," *Molecular Cell*, vol. 26, no. 1, pp. 1–14, 2007.

[6] R. D. Nagarajan, P. Murugan, K. Palaniyandi, R. Atchudan, and A. K. Sundramoorthy, "Biocompatible MXene (Ti3C2Tx) immobilized with flavin adenine dinucleotide as an electrochemical transducer for hydrogen peroxide detection in ovarian cancer cell lines," *Micromachines*, vol. 12, no. 8, p. 862, 2021.

[7] B. Halliwell, M. V. Clement, and L. H. Long, "Hydrogen peroxide in the human body," *FEBS Letters*, vol. 486, no. 1, pp. 10–13, 2000.

[8] M. Peng, Y. Zhao, D. Chen, and Y. Tan, "Free-standing 3D electrodes for electrochemical detection of hydrogen peroxide," *ChemCatChem*, vol. 11, no. 17, pp. 4222–4237, 2019.

[9] B. E. Watt, A. T. Proudfoot, and J. A. Vale, "Hydrogen peroxide poisoning," *Toxicological Reviews*, vol. 23, no. 1, pp. 51–57, 2004.

[10] C. Lennicke, J. Rahn, R. Lichtenfels, L. A. Wessjohann, and B. Seliger, "Engineering synthetic antibody binders for allosteric inhibition of prolactin receptor signaling," *Signals*, vol. 13, no. 1, pp. 1–19, 2015.

[11] R. F. P. Nogueira, M. C. Oliveira, and W. C. Paterlini, "Simple and fast spectrophotometric determination of H_2O_2 in photo-Fenton reactions using metavanadate," *Talanta*, vol. 66, no. 1, pp. 86–91, 2005.

[12] S. Singh, K. Mitra, R. Singh et al., "Colorimetric detection of hydrogen peroxide and glucose using brominated graphene," *Analytical Methods*, vol. 9, no. 47, pp. 6675–6681, 2017.

[13] R. Tian, B. Zhang, M. Zhao et al., "Fluorometric enhancement of the detection of H2O2 using different organic substrates and a peroxidase-mimicking polyoxometalate," *RSC Advances*, vol. 9, no. 22, pp. 12209–12217, 2019.

[14] J. G. Manjunatha, B. K. Swamy, M. Deraman, and G. P. Mamatha, "Simultaneous determination of ascorbic acid, dopamine and uric acid at poly (aniline blue) modified carbon paste electrode: a cyclic voltammetric study," *International Journal of Pharmacy and Pharmaceutical Sciences*, vol. 5, pp. 355–362, 2013.

[15] N. Hareesha and J. G. Manjunatha, "Elevated and rapid voltammetric sensing of riboflavin at poly(helianthin dye) blended carbon paste electrode with heterogeneous rate constant elucidation," *Journal of the Iranian Chemical Society*, vol. 17, no. 6, pp. 1507–1519, 2020.

[16] J. Ju and W. Chen, "In situ growth of surfactant-free gold nanoparticles on nitrogen-doped graphene quantum dots for electrochemical detection of hydrogen peroxide in biological environments," *Analytical Chemistry*, vol. 87, no. 3, pp. 1903–1910, 2015.

[17] M. Preethika and A. K. Sundramoorthy, "Humic acid/halloysite nanotube/flavin adenine dinucleotide nanocomposite based selective electrochemical biosensor for hydrogen peroxide," *Applied Surface Science*, vol. 488, pp. 503–511, 2019.

[18] P. Murugan, A. K. Sundramoorthy, D. Ganapathy, R. Atchudan, D. Nallaswamy, and A. Khosla, "Electrochemical detection of H2O2 using an activated glassy carbon electrode," *ECS Sensors Plus*, vol. 1, no. 3, article 034401, 2022.

[19] S. M. M. Raj, R. Atchudan, D. Ganapathy, A. Khosla, and A. K. Sundramoorthy, "Review—recent trends on the synthesis and different characterization tools for MXenes and their emerging applications," *Journal of the Electrochemical Society*, vol. 169, no. 7, article 077501, 2022.

[20] A. C. Carpenter, I. T. Paulsen, and T. C. Williams, "Blueprints for biosensors: design, limitations, and applications," *Genes*, vol. 9, no. 8, p. 375, 2018.

[21] G. Jeevanandham, R. Jerome, N. Murugan, M. Preethika, K. Vediappan, and A. K. Sundramoorthy, "Nickel oxide decorated MoS2 nanosheet-based non-enzymatic sensor for the selective detection of glucose," *RSC Advances*, vol. 10, no. 2, pp. 643–654, 2020.

[22] S. Majumder, B. Saha, S. Dey, R. Mondal, S. Kumar, and S. Banerjee, "A highly sensitive non-enzymatic hydrogen peroxide and hydrazine electrochemical sensor based on 3D micro-snowflake architectures of α-Fe2O3," *RSC Advances*, vol. 6, no. 65, pp. 59907–59918, 2016.

[23] T. Liu, Y. Guo, Z. Zhang, Z. Miao, X. Zhang, and Z. Su, "Fabrication of hollow CuO/PANI hybrid nanofibers for non-enzymatic electrochemical detection of H_2O_2 and glucose," *Sensors and Actuators B: Chemical*, vol. 286, pp. 370–376, 2019.

[24] M. Baghayeri, H. Alinezhad, M. Tarahomi, M. Fayazi, M. Ghanei-Motlagh, and B. Maleki, "A non-enzymatic hydrogen peroxide sensor based on dendrimer functionalized magnetic graphene oxide decorated with palladium nanoparticles," *Applied Surface Science*, vol. 478, pp. 87–93, 2019.

[25] A. K. Sundramoorthy, S. Mesgari, J. Wang et al., "Scalable and effective enrichment of semiconducting single-walled carbon nanotubes by a dual selective naphthalene-based azo dispersant," *Journal of the American Chemical Society*, vol. 135, no. 15, pp. 5569–5581, 2013.

[26] G. Tigari and J. G. Manjunatha, "Electrochemical preparation of poly(arginine)-modified carbon nanotube paste electrode and its application for the determination of pyridoxine in the presence of riboflavin: an electroanalytical approach," *Journal of Analysis and Testing*, vol. 3, no. 4, pp. 331–340, 2019.

[27] C. Raril and J. G. Manjunatha, "Fabrication of novel polymer-modified graphene-based electrochemical sensor for the determination of mercury and lead ions in water and biological samples," *Journal of Analytical Science and Technology*, vol. 11, no. 1, pp. 1–10, 2020.

[28] J. G. Manjunatha, "A surfactant enhanced graphene paste electrode as an effective electrochemical sensor for the sensitive and simultaneous determination of catechol and resorcinol," *Chemical Data Collections*, vol. 25, article 100331, 2020.

[29] N. Hareesha and J. G. Manjunatha, "Fast and enhanced electrochemical sensing of dopamine at cost-effective poly(DL-phenylalanine) based graphite electrode," *Journal of Electroanalytical Chemistry*, vol. 878, article 114533, 2020.

[30] N. G. Yasri, A. K. Sundramoorthy, W.-J. Chang, and S. Gunasekaran, "Highly selective mercury detection at partially oxidized graphene/poly(3,4-ethylenedioxythiophene):poly(styrenesulfonate) nanocomposite film-modified electrode," *Frontiers in Materials*, vol. 1, p. 33, 2014.

[31] T. H. V. Kumar, S. K. Yadav, and A. K. Sundramoorthy, "Review-electrochemical synthesis of 2D layered materials and their potential application in pesticide detection," *Journal of the Electrochemical Society*, vol. 165, no. 16, pp. B848–B861, 2018.

[32] T. H. V. Kumar and A. K. Sundramoorthy, "Electrochemical biosensor for methyl parathion based on single-walled carbon nanotube/glutaraldehyde crosslinked acetylcholinesterase-wrapped bovine serum albumin nanocomposites," *Analytica Chimica Acta*, vol. 1074, pp. 131–141, 2019.

[33] A. M. Dimiev, A. Khannanov, I. Vakhitov, A. Kiiamov, K. Shukhina, and J. M. Tour, "Revisiting the mechanism of oxidative unzipping of multiwall carbon nanotubes to graphene nanoribbons," *ACS Nano*, vol. 12, no. 4, pp. 3985–3993, 2018.

[34] M. Fujita, K. Wakabayashi, K. Nakada, and K. Kusakabe, "Peculiar localized state at zigzag graphite edge," *Journal of the Physical Society of Japan*, vol. 65, no. 7, pp. 1920–1923, 1996.

[35] Y.-W. Son, M. L. Cohen, and S. G. Louie, "Half-metallic graphene nanoribbons," *Nature*, vol. 444, no. 7117, pp. 347–349, 2006.

[36] J. Bai, X. Duan, and Y. Huang, "Rational fabrication of graphene nanoribbons using a nanowire etch mask," *Nano Letters*, vol. 9, no. 5, pp. 2083–2087, 2009.

[37] V. Abramova, A. S. Slesarev, and J. M. Tour, "Meniscus-mask lithography for fabrication of narrow nanowires," *Nano Letters*, vol. 15, no. 5, pp. 2933–2937, 2015.

[38] J. Cai, P. Ruffieux, R. Jaafar et al., "Atomically precise bottom-up fabrication of graphene nanoribbons," *Nature*, vol. 466, no. 7305, pp. 470–473, 2010.

[39] T. H. Vo, M. Shekhirev, D. A. Kunkel et al., "Large-scale solution synthesis of narrow graphene nanoribbons," *Nature Communications*, vol. 5, no. 1, pp. 1–8, 2014.

[40] A. G. Cano-Márquez, F. J. Rodriguez-Macias, J. Campos-Delgado et al., "Ex-MWNTs: graphene sheets and ribbons produced by lithium intercalation and exfoliation of carbon nanotubes," *Nano Letters*, vol. 9, no. 4, pp. 1527–1533, 2009.

[41] D. V. Kosynkin, W. Lu, A. Sinitskii, G. Pera, Z. Sun, and J. M. Tour, "Highly conductive graphene nanoribbons by longitudinal splitting of carbon nanotubes using potassium vapor," *ACS Nano*, vol. 5, no. 2, pp. 968–974, 2011.

[42] D. V. Kosynkin, A. L. Higginbotham, A. Sinitskii et al., "Longitudinal unzipping of carbon nanotubes to form graphene nanoribbons," *Nature*, vol. 458, no. 7240, pp. 872–876, 2009.

[43] Y. Zhu, Z. Sun, Z. Yan, Z. Jin, and J. M. Tour, "Rational design of hybrid graphene films for high-performance transparent electrodes," *ACS Nano*, vol. 5, no. 8, pp. 6472–6479, 2011.

[44] A.-R. O. Raji, R. Villegas Salvatierra, N. D. Kim et al., "Lithium batteries with nearly maximum metal storage," *ACS Nano*, vol. 11, no. 6, pp. 6362–6369, 2017.

[45] B. Genorio, W. Lu, A. M. Dimiev et al., "In situ intercalation replacement and selective functionalization of graphene nanoribbon stacks," *ACS Nano*, vol. 6, no. 5, pp. 4231–4240, 2012.

[46] H. Chen, N. Bucher, S. Hartung et al., "A multi-walled carbon nanotube core with graphene oxide nanoribbon shell as anode material for sodium ion batteries," *Advanced Materials Interfaces*, vol. 3, no. 20, p. 1600357, 2016.

[47] R. John, D. B. Shinde, L. Liu et al., "Sequential electrochemical unzipping of single-walled carbon nanotubes to graphene ribbons revealed by in situ Raman spectroscopy and imaging," *ACS Nano*, vol. 8, no. 1, pp. 234–242, 2014.

[48] S. Vadahanambi, J.-H. Jung, R. Kumar, H.-J. Kim, and I.-K. Oh, "An ionic liquid-assisted method for splitting carbon nanotubes to produce graphene nano-ribbons by microwave radiation," *Carbon*, vol. 53, pp. 391–398, 2013.

[49] F. Cataldo, G. Compagnini, G. Patané et al., "Graphene nanoribbons produced by the oxidative unzipping of single-wall carbon nanotubes," *Carbon*, vol. 48, no. 9, pp. 2596–2602, 2010.

[50] A. Martín, J. Hernández-Ferrer, M. T. Martínez, and A. Escarpa, "Graphene nanoribbon-based electrochemical sensors on screen-printed platforms," *Electrochimica Acta*, vol. 172, pp. 2–6, 2015.

[51] L. Zhu, L. Kong, and C. Zhang, "Numerical study on hysteretic behaviour of horizontal-connection and energy-dissipation structures developed for prefabricated shear walls," *Applied Sciences*, vol. 10, no. 4, p. 1240, 2020.

[52] X. Huang, Y. Zhu, and E. Kianfar, "Nano biosensors: properties, applications and electrochemical techniques," *Journal of Materials Research and Technology*, vol. 12, pp. 1649–1672, 2021.

[53] W. Jia, M. Guo, Z. Zheng et al., "Electrocatalytic oxidation and reduction of H2O2 on vertically aligned Co3O4 nanowalls electrode: toward H_2O_2 detection," *Journal of Electroanalytical Chemistry*, vol. 625, no. 1, pp. 27–32, 2009.

[54] C. L. Bentley, M. Kang, and P. R. Unwin, "Nanoscale surface structure–activity in electrochemistry and electrocatalysis," *Journal of the American Chemical Society*, vol. 141, no. 6, pp. 2179–2193, 2019.

[55] M. A. Shenashen, D. Hassen, S. A. El-Safty, H. Isago, A. Elmarakbi, and H. Yamaguchi, "Axially oriented tubercle vein and X-crossed sheet of N-Co_3O_4@C hierarchical mesoarchitectures as potential heterogeneous catalysts for methanol oxidation reaction," *Chemical Engineering Journal*, vol. 313, pp. 83–98, 2017.

[56] Q. Shu, Z. Xia, W. Wei et al., "Controllable unzipping of carbon nanotubes as advanced Pt catalyst supports for oxygen reduction," *ACS Applied Energy Materials*, vol. 2, no. 8, pp. 5446–5455, 2019.

[57] R. D. Nagarajan and A. K. Sundramoorthy, "One-pot electrosynthesis of silver nanorods/graphene nanocomposite using 4-sulphocalix[4]arene for selective detection of oxalic acid," *Sensors and Actuators B: Chemical*, vol. 301, article 127132, 2019.

[58] S. Farhadi, M. Javanmard, and G. Nadri, "Characterization of cobalt oxide nanoparticles prepared by the thermal decomposition," *Acta Chimica Slovenica*, vol. 63, no. 2, pp. 335–343, 2016.

[59] M. Liu, Y. Du, Y.-E. Miao et al., "Anisotropic conductive films based on highly aligned polyimide fibers containing hybrid materials of graphene nanoribbons and carbon nanotubes," *Nanoscale*, vol. 7, no. 3, pp. 1037–1046, 2015.

[60] V. Sahu, S. Shekhar, R. K. Sharma, and G. Singh, "Ultrahigh performance supercapacitor from lacey reduced graphene oxide nanoribbons," *ACS Applied Materials & Interfaces*, vol. 7, no. 5, pp. 3110–3116, 2015.

[61] B. Sidhureddy, J. S. Dondapati, and A. Chen, "Shape-controlled synthesis of Co3O4 for enhanced electrocatalysis of the oxygen evolution reaction," *Chemical Communications*, vol. 55, no. 25, pp. 3626–3629, 2019.

[62] K. Białas, D. Moschou, F. Marken, and P. Estrela, "Electrochemical sensors based on metal nanoparticles with biocatalytic activity," *Microchimica Acta*, vol. 189, no. 4, p. 172, 2022.

[63] Z. Fan, Q. Lin, P. Gong, B. Liu, J. Wang, and S. Yang, "A new enzymatic immobilization carrier based on graphene capsule for hydrogen peroxide biosensors," *Electrochimica Acta*, vol. 151, pp. 186–194, 2015.

[64] M. A. Karimi, F. Banifatemeh, A. Hatefi-Mehrjardi, H. Tavallali, Z. Eshaghia, and G. Deilamy-Rad, "A novel rapid synthesis of Fe_2O_3/graphene nanocomposite using ferrate(VI) and its application as a new kind of nanocomposite modified

electrode as electrochemical sensor," *Materials Research Bulletin*, vol. 70, pp. 856–864, 2015.

[65] L. Kong, Z. Ren, N. Zheng et al., "Interconnected 1D Co3O4 nanowires on reduced graphene oxide for enzymeless H2O2 detection," *Nano Research*, vol. 8, no. 2, pp. 469–480, 2015.

[66] A. A. Ensafi, M. Jafari–Asl, and B. Rezaei, "A novel enzyme-free amperometric sensor for hydrogen peroxide based on Nafion/exfoliated graphene oxide- Co_3O_4 nanocomposite," *Talanta*, vol. 103, pp. 322–329, 2013.

[67] P. Murugan, J. Annamalai, R. Atchudan et al., "Electrochemical sensing of glucose using glucose oxidase/PEDOT: 4-sulfocalix [4] arene/MXene composite modified electrode," *Micromachines*, vol. 13, no. 2, p. 304, 2022.

[68] B. P. Vinayan and S. Ramaprabhu, "Facile synthesis of SnO2 nanoparticles dispersed nitrogen doped graphene anode material for ultrahigh capacity lithium ion battery applications," *Journal of Materials Chemistry A*, vol. 1, no. 12, pp. 3865–3871, 2013.

[69] C. Liu, C. Li, K. Ahmed et al., "High energy and power density Li–O2 battery cathodes based on amorphous RuO2 loaded carbon free and binderless nickel nanofoam architectures," *RSC Advances*, vol. 6, no. 85, pp. 81712–81718, 2016.